Biostratigraphy of large benthic foraminifera from Hole U1468A (Maldives): a CT-scan taxonomic approach

Giovanni Coletti[1] · Stephanie Stainbank[1] · Alessio Fabbrini[2] · Silvia Spezzaferri[1] · Anneleen Foubert[1] · Dick Kroon[3] · Christian Betzler[4]

Abstract
Large benthic foraminifera are important components of tropical shallow water carbonates. Their structure, developed to host algal symbionts, can be extremely elaborate and presents stratigraphically-significant evolutionary patterns. Therefore their distribution is important in biostratigraphy, especially in the Indo-Pacific area. To provide a reliable age model for two intervals of IODP Hole U1468A from the Maldives Inner-Sea, large benthic foraminifera have been studied with computed tomography. This technique provided 3D models ideal for biometric-based identifications, allowing the upper interval to be placed in the late middle-Miocene and the lower interval in the late Oligocene.

Keywords Microtomography · *Nephrolepidina* · *Cycloclypeus* · *Heterostegina* · *Amphistegina* · Nummulitids

1 Introduction

Large Benthic Foraminifera (LBF) are important component in tropical carbonate platforms, major sediment producers and powerful tools for stratigraphic and environmental studies (Hottinger 1977; 1983; Schaub 1981; Lee and Hallock 1987; Pignatti et al. 1998; Serra-Kiel et al. 1998; Beavington-Penney and Racey 2004; Boudagher-Fadel 2008). Their tests present complex internal architectures, related to the presence of algal symbionts, that coupled with their external morphology, are fundamental for their taxonomy (Tan 1932; Loeblich and Tappan 1964; Haynes 1965; Hottinger 1977). Their distribution is controlled by temperature, light intensity, water energy, substrate type, nutrient availability and detrital input (Hohenegger 1994, 2000; Langer and Hottinger 2000; Renema et al. 2001; Beavington-Penney and Racey 2004; Renema 2007, 2018). LBF are particularly common and diverse in the Indo-Pacific, where, from the Paleogene to present-day, they massively contributed to carbonate production (Hallock 1981; Tudhope and Scoffin 1988; Renema et al. 2001; Renema 2006). Because of their high abundance, stratigraphy based on LBF represents a powerful dating tool (Van der Vlerk and Umbgrove 1927; Adams 1970; Chaproniere 1984; Boudagher-Fadel and Banner 1999; Boudagher-Fadel and Lokier 2005; Renema 2007). However, the correlation between carbonate platforms and the adjacent basin is challenging when independent age-controls are not available. LBF lineages can be regional, leading to further problems (Renema 2015). Specimen preparation is problematic in itself since perfectly oriented thin sections are necessary for reliable identifications (Briguglio et al. 2014). This approach is time consuming and destructive, making it impossible to obtain axial and equatorial sections of the same specimen (Briguglio et al. 2013). Computed tomographic scanner (CT-scan) overcomes these limitations, giving 3D

Editorial handling: D. Marty.

Electronic supplementary material The online version of this article (https://doi.org/10.1007/s00015-018-0306-7) contains supplementary material, which is available to authorized users.

✉ Giovanni Coletti
giovanni.p.m.coletti@gmail.com

[1] Department of Geosciences, University of Fribourg, Chemin du Musée 6, 1700 Fribourg, Switzerland

[2] Department of Physical Sciences, Earth and Environment, University of Siena, Strada Laterina 8, 53100 Siena, Italy

[3] School of GeoSciences, University of Edinburgh, Grant Institute, The King's Buildings, James Hutton Road, EH9 3FE Edinburgh, UK

[4] Institute of Geology, CEN, University of Hamburg, Bundesstrasse 55, 20146 Hamburg, Germany

representations of both external and internal structures along every possible section (e.g., Benedetti and Briguglio 2012; Hohenegger and Briguglio 2014; Briguglio and Hohenegger 2014; Briguglio et al. 2016).

Aim of this study is to provide a preliminary biostratigraphy for two intervals from Hole U1468A, drilled by the International Ocean Discovery Program (IODP) in the Inner Maldivian Sea, using LBF assemblages. Species identification follows a morphometric approach based on the results of the CT-scanning. Obtained ages are correlated with planktonic foraminifera and nannofossil distributions to provide independent age controls.

2 Geological setting

The Maldivian archipelago is a pure carbonate depositional system composed of two rows of atolls, separated by channels and surrounding the Inner Sea (Fig. 1; Aubert and Droxler 1996). Carbonate platforms surround the atolls, while periplatform ooze sedimentation, locally accumulating as drift deposits, occur in the Inner Sea (Droxler et al. 1990; Betzler et al. 2013). The sedimentation started between the early Eocene and Oligocene. At first it was restricted to narrow bands on the oceanward areas, leading to the formation of a double row of atolls. Subsequently, platform margins prograded toward the Inner Sea and current-related, clinoform bodies characterized the region from the late middle-Miocene (Betzler et al. 2017). In one of the channels connecting the Inner Sea to the ocean, IODP Expedition 359 drilled Hole U1468A (4°55.98′N, 73°4.28′E, water depth of 521 m; Fig. 1). The recovered succession features eight units, among them Units II, VII and VIII are characterized by shallow-water carbonates and a rich LBF fauna (Unit II, 45.7–192.5 mbsf, 6H–30F; Unit VII, 817.5–854.7 mbsf, 106X–109X; Unit VIII, 854.7–865 mbsf, 110X–111X; Betzler et al. 2017).

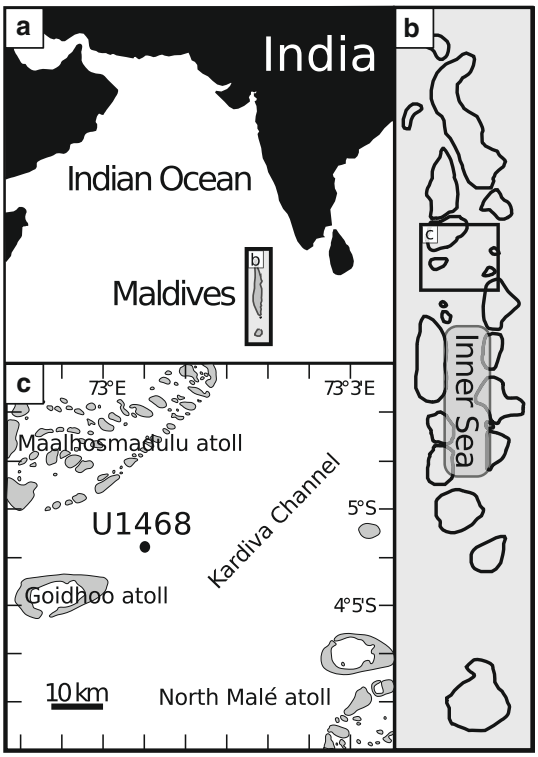

Fig. 1 Location map of Site U1468 in the Maldivian Inner Sea (after Betzler et al. 2017)

3 Methods

The first analyzed interval includes four regularly spaced samples spanning Unit II: 29F-CC; 22F-CC; 15F-CC and 7H-CC. The second interval consists of four samples covering Units VII-VIII: 110X-CC; 109X-CC; 108X-CC and 107X-CC. Samples were soaked in water, then washed through a 32 μm sieve and dried. In each sample LBF were selected, based on their external morphology, to represent the entire assemblage. 160 specimens were mounted with standard clear nail polish at distinct levels, 5 mm apart, around cylindrical Polyether ether ketone (PEEK) sample holders (Distrelec stock no. 148-21-756). Sample holders, manufactured in-house, were 6 cm in length, comprising a 5 cm length shaft (4 mm of diameter) and a 1 cm length base (6.4 mm of diameter; Fig. 2). The base serves for easy mounting into the Bruker SP-1212 and SP-1213 CT stage extenders. The shaft allowed the fixation of 5–8 specimens at each level, depending on size (Fig. 2). Similarly sized individuals were mounted at each level (Fig. 2). Specimens were scanned with a multi-scaled Bruker X-ray nano-computer tomographic scanner SkyScan 2211, using an open X-ray source with a diamond-window target at energies of 60 kV and currents of 350 μA. Images were acquired on a 11Mp cooled CCD detector resulting in a voxel resolution of 2 μm. 180° scans were taken with a rotation step of 1° (25′ of acquisition time for each level). Images were subsequently reconstructed with InstaRecon applying Gaussian smoothing, beam hardening and ring artifact corrections. Reconstructed images were analyzed with CTAn, CTVox and Avizo (FEI). After scanning, LBF specimens were removed from the PEEK sample holders with acetone.

The biometric study focused on equatorial sections integrating different procedures proposed in literature (Fig. 3; Tan 1932; Van der Vlerk 1959, 1963; O'Herne 1972; Matteucci and Schiavinotto 1977; Van Vessem 1978; Schiavinotto 1978; Chaproniere 1980; Hohenegger et al. 2000; Less et al. 2008; Özcan et al. 2009; Hohenegger 2011; Renema 2015; Benedetti et al. 2017; Torres-Silva

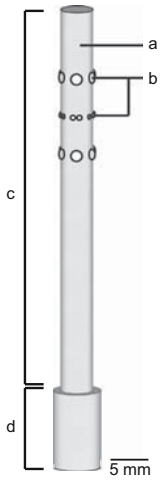

Fig. 2 PEEK sample holders for LBF CT-scanning. **a** PEEK rod **b** LBF mounted around the PEEK rod, in distinct intervals, with standard nail polish **c** sample holder shaft and **d** base

et al. 2017). Species identifications were mostly based on biometric parameters. Following Özcan et al. (2009), the notation exemplum intercentrale (ex. interc.) was used whenever the mean value of the identifying parameter of a group of specimens fell very close to the limits of two contiguous species of the same lineage. The complete biometric dataset is provided online (Online resources 1–4).

4 Systematic paleontology

Family Lepidocyclinidae Scheffen 1932

Genus *Nephrolepidina* Douville 1911

Test discoidal, biconvex with a distinct layer of equatorial chambers and lateral chambers on each side. Megalospheric stage with a protoconch only partially embrached by the deuteroconch.

Nephrolepidina ex. interc. *rutteni* Van der Vlerk 1924 -*martinii* Schlumberger 1900; Fig. 4a–n; Online resource 1.

Test biconvex, symmetrical and rounded. Surface with common, randomly distributed pustules representing the outer termination of thick pillars. Remnants of a collar can be observed along the equatorial plane. Embryo of megalospheric specimens small (PW = 105 μm; DW = 185 μm), with a rounded to slightly rectangular protoconch which is largely embraced by the deuteroconch (Ai = 61%). The wall enclosing the embryo is thick, while the wall dividing the two initial chambers is thin. No ACI observed on the protoconch, NPAC = 2. External surface of the deuteroconch almost completely covered by ACII (NACII = 6.3). Chambers on the equatorial plane disposed in a wavy concentric pattern (F = 4).

Remarks: The average number of ACII observed in the examined specimens suggests a positioning between *N. martini* (6.5 > NACII>4.5) and *N. rutteni* (NACII > 6.5; Van Vessem 1978). No remarkable variability observed among the samples, B∑ACII is rather constant.

Nephrolepidina transiens Umbgrove 1929; Fig. 4o.

Test biconvex, symmetrical and rounded. Surface with common, randomly distributed pustules. Remnants of a collar can be observed along the equatorial plane. Embryo of megalospheric specimens large (PW > 250 μm; DW > 350 μm), with an irregularly shaped deuteroconch. Wall of the embryo thick and surrounded by a large number of irregularly-shaped auxiliary chambers. Equatorial chambers disposed in a wavy concentric pattern (F = 4).

Nephrolepidina ex. interc. *isolepidinoides* Van der Vlerk 1929 -*sumatrensis* Brady 1875; Fig. 4 p–x; Online resource 1.

Test biconvex, symmetrical and rounded. Surface characterized by common pustules. Remnants of a collar can be observed along the outer surface of the equatorial plane. Embryo small (PW = 130 μm; DW = 200 μm), composed of a rounded protoconch and a kidney-shaped deuteroconch, the latter only slightly encloses the protoconch (Ai = 43%). Wall enclosing the embryo as thick as the wall separating the first and second chambers. NPAC = 2 and NACII = 1.8, no ACI observed. Chambers on the equatorial plane disposed with an intersecting curve pattern (F = 1).

Remarks: The low NACII observed in this population, coupled with the low Ai value, places these specimens between *N. isolepidinoides* and *N. sumatrensis*. The former is characterized by an Ai < 40% and NACII < 2.25, while the latter has an Ai > 40% and NACII > 2.25 (Van Vessem 1978). Both Ai and NACII are higher in the specimens from 107X-CC and lower in those from 108X-CC.

Family Nummulitidae De Blainville 1827

Genus *Cycloclypeus* Carpenter 1856

Test large, circular, with a central umbo and a narrow periphery. Megalospheric stage has a central embryo composed of two chambers followed by a short nepionic spire composed at first by undivided chambers and then by chambers divided into chamberlets by secondary septula. This nepionic spire is followed by annular chambers divided into chamberlets.

Cycloclypeus annulatus Martin 1880; Fig. 5a–i; Online resource 2.

Test large and flat, with a central area surrounded by annular inflations as thick as the umbo (the test between the annuli is thin and fragile). Outer surface lacking evident ornamentations. Embryo consisting of a circular protoconch and a large kidney-shaped deuteroconch (PW = 195 μm; DW = 245 μm). The first two chambers are followed by a third undivided chamber (X = 3) and this entire structure is surrounded by a thick wall. The wall separating the three chambers from each other is thin. Specimens

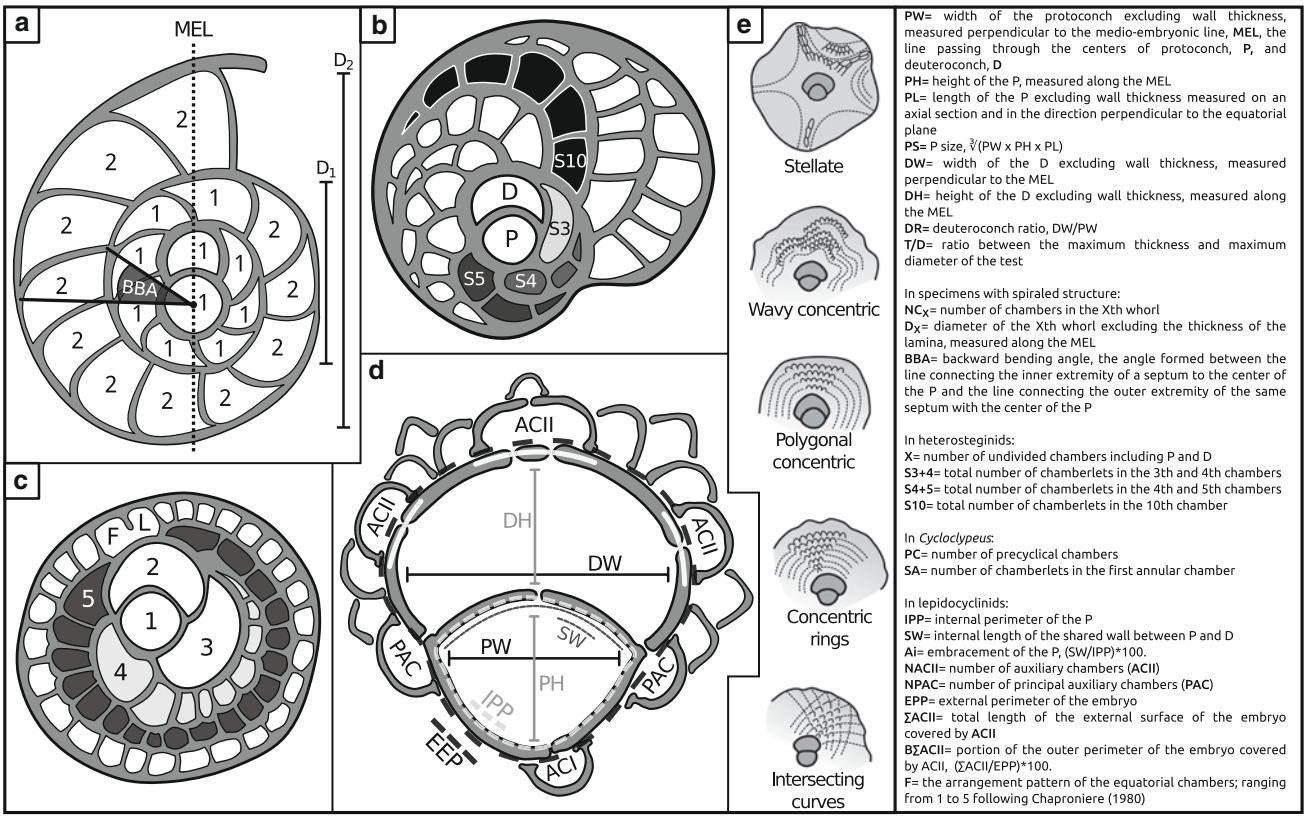

Fig. 3 biometry of LBF megalospheres. **a** Schematic drawing of a nummulitids, modified from Matteucci and Schiavinotto (1980); 1 marks the chambers of the first whorl; 2 marks the chambers of the second whorl; D_1 = diameter of the first whorl; D_2 = diameter of the second whorl. **b** Schematic drawing of an *Heterostegina*; X = 3, S3 + 4 = 4, S4 + 5 = 6 and S10 = 6. **c** Schematic drawing of a *Cycloclypeus*, modified from O'Herne (1972); FL = FL chamberlet of the first annular chamber; Y = 5 and SA = 27. **d** Schematic drawing of a *Nephrolepidina* embryo, modified from Van Vessem (1978); ACI = accessory auxiliary chambers of the protoconch. **e** Arrangement patter of equatorial chambers in *Nephrolepidina*, modified from Van Vessem (1978) and Chaproniere (1980); Stellate: F = 5; Wavy concentric: F = 4; Polygonal concentric: F = 3; Concentric rings: F = 2; Intersecting curves: F = 1

generally characterized by 7 to 8 precyclical chambers (PC = 7.8; S4 + 5= 10.7).

Cycloclypeus eidae Tan 1930; Fig. 5j–n.

Specimens poorly preserved, broken and bioturbated. Test large and flat thicker at the center and thinner towards the edges. Outer surface granulated. Embryo composed of a small and rounded protoconch (PW 70 to 90 μm) and a hemispherical deuteroconch. One or two undivided chambers (X ≈ 3–4) and two whorls of nepionic chambers follow the embryo, after which annular growth starts.

Genus *Heterostegina* D'Orbigny 1826

Subgenus *Vlerkina* Eames, Clarke, Banner, Smout and Blow 1968 emended Banner and Hodgkinson 1991.

Test lenticular, biconvex, planispiral and involute. Embryo of megalospheric specimens composed of two chambers, followed by a variable number of undivided chambers. Later chambers are divided into chamberlets by secondary septula. Alar prolongations generally subdivided into lateral chamberlets. In axial section it present a single layer of lateral chamberlets is present for each whorl of the spire.

Heterostegina (*Vlerkina*) *borneensis* Van der Vlerk 1930; Fig. 5o–x; Online resource 3.

Test, involute, planispiral, flat and thicker at the center. Some specimens seems to have pillars in the central part of the test, but the external surface is generally abraded and bioturbated, therefore, it is unclear whether or not ornamentations were present. Alar prolongations are narrow and divide into a single layer of lateral chamberlets. Embryo large and composed of a rounded protoconch followed and a kidney-shaped deuteroconch (PW = 210 μm; DW = 250 μm). This structure is followed by one undivided chamber (X = 3; S3 + 4= 3.9; S4 + 5= 7; S10 = 7).

Heterostegina (*Vlerkina*) sp. 1; Fig. 6a–g; Online resource 3.

Test large, planispiral, involute and thick. Outer surface unornamented. Alar prolongations narrow and divided into lateral chamberlets. A single layer of lateral chamberlets is present for each whorl. Protoconch and deuteroconch small; two to three undivided chambers follow them (PW = 105 μm; DW = 110 μm; X = 5.5). Compared to

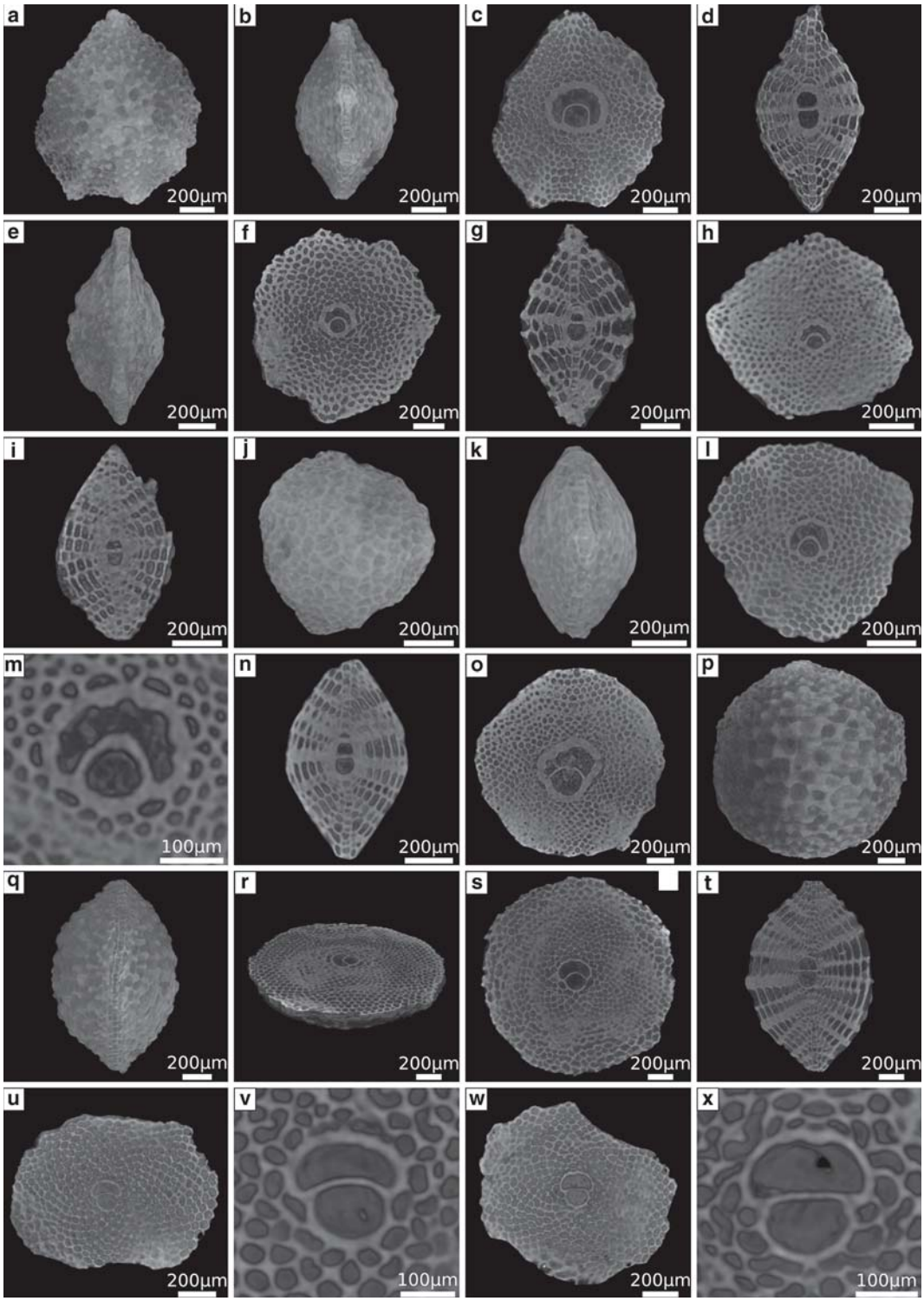

Fig. 4 *Nephrolepidina* ex. interc. *ruttenii- martini* in panels **a**–**n**, *Nephrolepidina transiens* in panel **o**, *Nephrolepidina* ex. interc. *isolepidinoides-sumatrensis* in panels **p**–**x**. **a** External axial view of a specimen 7_1_07. **b** External equatorial view of 7_1_07. **c** Equatorial section of 7_1_07, a perfect *N. ruttenii* end-member of the population. **d** Axial section of 7_1_07. **e** External axial view of 29_3_05. **f** Equatorial section of 29_3_05. **g** Axial section of 29_3_05. **h** Equatorial section of 29_3_02, a perfect *N. martini* end-member of the population. **i** Axial section of 29_3_02. **j** External equatorial view of 29_5_01. **k** External axial view of 29_5_01. **l** Equatorial section of 29_5_01, an intermediate form of the population. **m** Detail of the embryo of 29_5_01. **n** Axial section of 29_5_01. **o** Equatorial section of 29_3_03. **p** External equatorial view of 107_2_00. **q** External axial view of 107_2_00. **r** Sectioned 3D model of 107_2_00. **s** Equatorial section of 107_2_00, a good example close to the *N. sumatrensis* type. **t** Axial section of 107_2_00. **u** Equatorial section of 108_2_09, a specimen with intermediate characteristics. **v** Detail of the embryo of 108_2_09. **w** Equatorial section of 108_2_10 which is closer to the *N. isolepidinoides* characteristics. **x** Detail of the embryo of 108_2_10

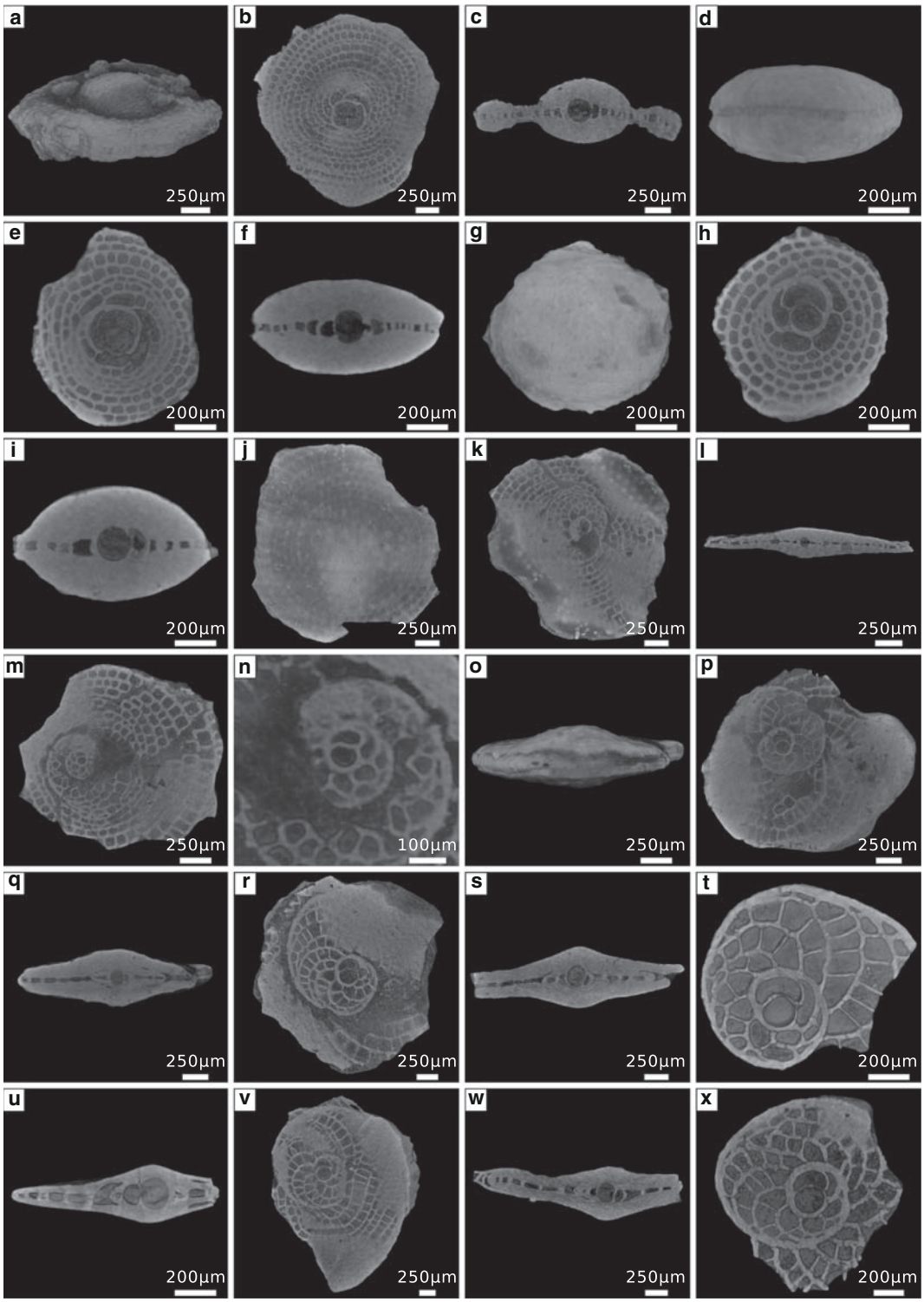

Fig. 5 *Cycloclypeus annulatus* panels **a**–**i**, *Cycloclypeus eidae* panels **j**–**n**, *Heterostegina (Vlerkina) borneensis* panels **o**–**x**. **a** External view of specimen 29_1_04A. **b** Equatorial section of 29_1_04A. **c** Axial section of 29_1_04A. **d** External view of the central part of 29_4_00, a specimen whose rings were lost. **e** Equatorial section of 29_4_00. **f** Axial section of 29_4_00. **g** External view of 29_5_04. **h** Equatorial section of 29_5_04. **i** Axial section of 29_5_04. **j** External view of 107_1_03A. **k** Equatorial section of 107_1_03A. **l** Axial section of 107_1_03A. **m** Equatorial section of 107_1_01. **n** Detail of the embryo of 107_1_01. **o** External view of 107_1_04. **p** Equatorial section of 107_1_04, the specimen is clearly micro-bored. **q** Axial section of 107_1_04. **r** Equatorial section of 109_1_04. **s** Axial section of 109_1_04. **t** Equatorial section of 109_1_08. **u** Axial section of 109_1_08. **v** Equatorial section of 109_3_04. **w** Axial section of 109_3_04. **x** Equatorial section of 109_2_05

H. (*V.*) *borneensis* the subsequent chambers have less subdivisions (S3 + 4= 2; S4 + 5= 2.8; S10 = 3.3).

Remarks: This species differs from *H. (V.) borneensis* by its smaller protoconch, more undivided chambers after the embryo, and less chamberlets in the first divided chambers. It also differs from other coeval *Heterostegina* (*Vlerkina*) species of the Indo-Pacific. The protoconch is smaller than both *Heterostegina* (*Vlerkina*) *pleurocentralis* and *Heterostegina* (*Vlerkina*) *assilinoides*, it has more undivided chambers and less chamberelets in the 3rd, 4th, 5th and 10th chambers of the spire (Banner and Hodgkinson 1991).

Genus *Operculina* D'Orbigny 1826

Test lenticular, planispiral, from evolute to almost completely involute, with a lax spire. Septa can be regular or folded and can present partially developed septula.

Operculina complanata (De France In Blainville 1822); Fig. 6i–q; Online resource 4.

Test planispiral, entirely evolute and very flat, with a granulated surface. Alar prolongations absent. Protoconch small and rounded (PW = 42 µm). Deuteroconch small and kidney-shaped (PW = 23 µm). Septa are quite regular and they do not have septula.

Operculina cf. *heterosteginoides*; Fig. 6h–k; Online resource 4.

Test planispiral, entirely evolute, very flat, with a smooth outer surface. Alar prolongations absent. Embryo small and composed of a rounded protoconch and a hemispherical deuteroconch (PW = 60 µm; DW = 60 µm). Subsequent chambers partially divided by incomplete septula.

Remarks: This species has a lax spire and fewer incomplete septula than the extant *Operculina heterosteginoides*. Evolute nummulitids with incomplete chamber divisions are have a complex taxonomic history (Renema 2018). Since their revision is beyond the purpose of this paper we simply compare this species with the extant *O. heterosteginoides*, the most similar living representative of the group.

Operculina sp.1; Fig. 6r–x; Online resource 4.

Test planispiral, moderately thick and involute with a smooth outer surface. Alar prolongations long and narrow. Embryo composed of a small rounded protoconch and kidney-shaped deuteroconch (PW = 35 µm; DW = 29 µm). Septa often bent and irregular as the main wall of the spire.

Nummulitidae sp. 1; Fig. 7a–f; Online resource 4.

Test planispiral, thick, lenticular and completely involute. Alar prolongation long and narrow, not extending over the center of the test. Embryo characterized by a small protoconch and a narrow, kidney-shaped, deuteroconch (PW = 48 µm; DW = 39 µm). Septa starting straight and slightly bending backwards close to the intersection with the wall of the subsequent whorl (BBA = 19).

Remarks: *Nummulites* and *Operculinella* are both involute nummilitids. They are distinguished mainly by shape of the last whorl (Hohenegger et al. 2000; Renema 2018). The presence of trabeculae on the surface is also considered important by some authors (Hohenegger et al. 2000), as well as the number of chambers in each whorl and the BBA (Hohenegger et al. 2000; Renema 2018). Since the examined specimens were always broken and abraded, estimate the number of chambers per whorl, studying the last whorl and the superficial features was unfeasible. Thus, straightforward species identification was impossible.

Family Amphisteginidae Cushman 1927

Genus *Amphistegina* D'Orbigny 1926

Test low trochospiral, involute to partially evolute and unevenly to almost uniformly biconvex. Chambers of the spire strongly curved backward at the periphery.

Amphistegina lessonii D'Orbigny 1926; Fig. 7h–m; Online resource 4.

Test trochospiral, involute, lenticular, slightly asymmetrical and thick, with a smooth surface. Alar prolongations long and narrow. Protoconch and deuteroconch very small (PW = 30 µm; DW = 22 µm). Chambers subdivided by strongly backward bending septa (BBA = 41). Coiling with a low expansion rate and few chambers per whorl.

Amphistegina mammilla (Fichtel and Moll 1798); Fig. 7n–u; Online resource 4.

Test trochospiral, involute, slightly to remarkably asymmetrical, moderately thick, with a smooth surface. Dorsal side more convex than the ventral side. Alar prolongations long and narrow. Protoconch spherical and small, deuteroconch small and hemispherical (PW = 42 µm; DW = 45 µm). Septa of the chambers strongly bending backwards (BBA= 55).

Family Acervulinidae Schultze 1854

Genus *Sphaerogypsina* Galloway 1933

Test globular to somewhat irregular. Constructed of numerous layers of polygonal to squared chambers arranged in column and radiating from the center. Outer surface characterized by a chessboard pattern of raised and depressed chambers. Embryo located at the center of the test, surrounded by an area of unordered chambers.

Sphaerogypsina sp. 1; Fig. 7v.

Test small and spherical, with a mean diameter of 800 µm. Outer surface displaying the characteristic chessboard pattern. Embryo small and trochospiral. Embryonic area followed by a few rings of unordered chambers, which in turn are surrounded by chambers arranged in a more or less regular pattern of radial columns.

Remarks: It is indistinguishable from *Sphaerogypsina globula*. The lack of clear characteristics to separate the

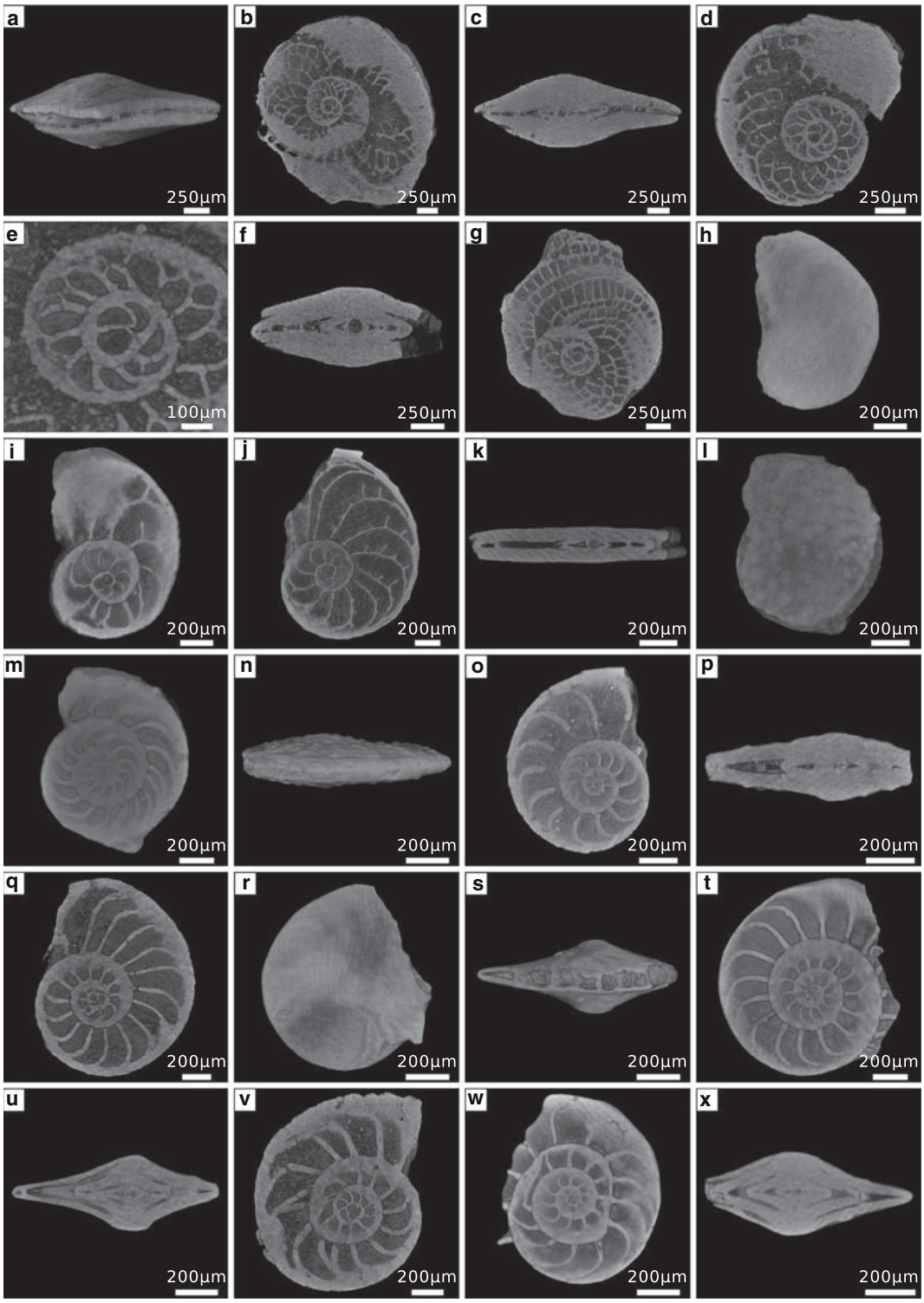

Fig. 6 *Heterostegina (Vlerkina)* sp. 1 panels **a–g**, *Operculina* cf. *heterosteginoides* panels **h–k**, *Operculina complanata* panels **i–q**, *Operculina* sp.1 panels **r–x**. **a** External view of 109_1_02. **b** Equatorial section of 109_1_02. **c** Axial section of 109_1_02. **d** Equatorial section of 109_1_00. **e** Detail of the embryo of 109_1_00. **f** Axial section of 109_1_00. **g** Equatorial section of 109_1_03. **h** External view of 107_2_04. **i** Equatorial section of 107_2_04. **j** Equatorial section of 107_2_06. **k** Axial section of 107_2_06. **l** External view of 29_2_04. **m** Equatorial section of 29_2_04. **n** External view of 109_1_07. **o** Equatorial section of 109_1_07. **p** Axial section of 109_1_07. **q** Equatorial section of 109_2_01. **r** External equatorial view of 108_2_11. **s** External axial view of 108_2_11. **t** Equatorial section of 108_2_11. **u** Axial section of 108_2_11. **v** Equatorial section of 109_2_02 which presents clearly bend septa. **w** Equatorial section of 108_1_07 which is characterized by an imperfect spiral. **x** Axial section of 108_1_07

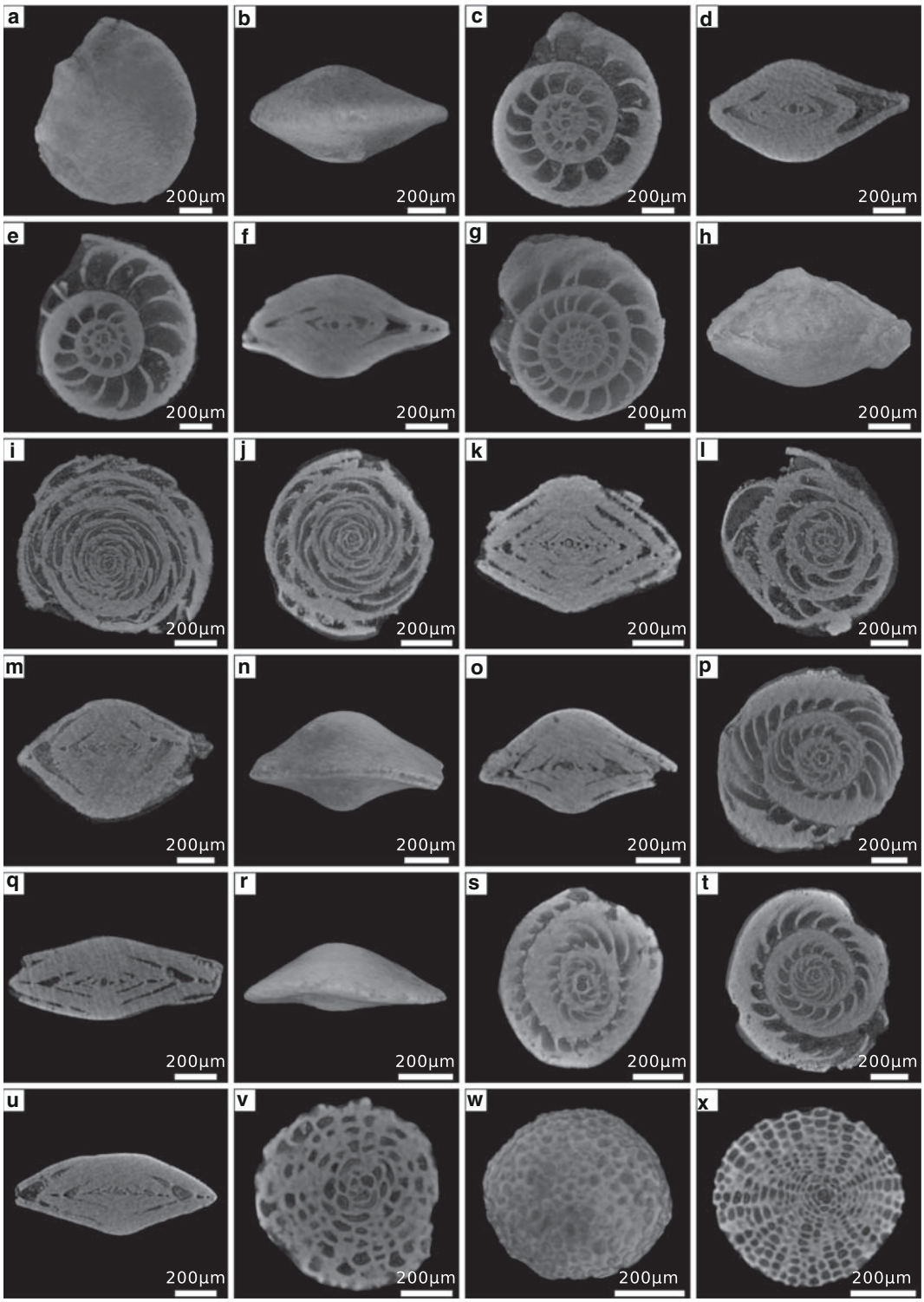

Fig. 7 Nummulitidae sp. 1 panels **a–f**, *Amphistegina lessonii* panels **h–m**, *Amphistegina mammilla* panels **n–u**, *Sphaerogypsina* sp.1 panel v, *Sphaerogypsina* sp. 2 panels **w–x**. **a** External equatorial view of 29_3_00. **b** External axial view of 29_3_00. **c** Equatorial section of 29_3_00. **d** Axial section of 29_3_00. **e** Equatorial section of 29_4_05. **f** Axial section of 29_4_05. **g** Equatorial section of 7_2_00. **h** External view of 22_3_00. **i** Equatorial section of 22_3_00. **j** Equatorial section of 22_1_06. **k** Axial section of 22_1_06. **l** Equatorial section of 22_1_00. **m** Axial section of 22_1_00. **n** External view of 107_2_03. **o** Axial section of 107_2_03. **p** Equatorial section of 107_2_02. **q** Axial section of 107_2_02. **r** External view of 108_1_06. **s** Equatorial section of 108_1_06. **t** Equatorial section of 107_3_02. **u** Axial section of 107_3_02. **v** Equatorial section of 29_5_03. **w** External view of 108_1_05. **x** Equatorial section of 108_1_05

species within this genus prevents an accurate identification.

Sphaerogypsina sp.2; Fig. 7w–x.

Test small and almost spherical (diameter of 750 μm). Outer surface exhibiting the characteristic chessboard pattern. Embryo bilocular, composed of a small elliptical protoconch and kidney-shaped deuteroconch. Embryonic area followed by a few rings of unordered chambers, which in turn are surrounded by chambers arranged in a regular pattern of radial columns.

Remarks: In contrast from *Sphaerogypsina* sp.1, it exhibits a bilocular embryo. Additionally, the radial column of chambers are more regularly arranged. Such a major differences clearly suggests that they are separated species and has substantial taxonomic implications. Since the taxonomy of *Sphaerogypsina* is beyond the purpose of this biostratigraphic paper the subject is not further investigated. *Sphaerogypsina* sp.2 also fits perfectly within the broad definition of *S. globula*, but the lack of clear characteristics for species separation prevents an accurate identification.

5 Discussion

5.1 Biostratigraphy

In the first interval (Unit II, Samples 7H-CC to 29F-CC), LBF specimens are poorly preserved with evidence of abrasion and fragmentation. The assemblage is quite uniform with *N.* ex. interc. *ruttenii-martinii* and *C. annulatus* occurring in all examined samples (the latter is particularly poorly preserved and many specimens only possess the central part of the test; Table 1). *Nephrolepidina*. ex. interc *martini-ruttenii* suggests at late middle-Miocene to early late-Miocene age (Adams 1970; Van Vessem 1978; Boudagher-Fadel 2002; Sharaf et al. 2005). Van Vessem's (1978) regards *N. ruttenii* as a more evolved species developing within the same lineage of *N. martini* and places this transition within Zone M11 (Wade et al. 2011). Chaproniere (1984) places these two species within the same lineage and their transition between Zones M9 and M10. Adams (1970) and Sharaf et al. (2005) consider *N. martini* and *N. ruttenii* two separate species, with overlapping stratigraphic ranges. For Adams (1970) *N. martini* is restricted to the middle Miocene while the range of *N. ruttenii* extends into the late Miocene. Sharaf et al. (2005) suggest a middle Miocene range for *N. martini* and an early to late Miocene range for *N. ruttenii*. The arrangement of equatorial chambers, which is stratigraphycally significant, supports a middle Miocene age (Chaproniere 1980; Betzler and Chaproniere 1993). Since the majority of the literature supports a M9 to M11 age for the examined *Nephrolepidina*, we will follow this line. *Cycloclypeus annulatus* ranges from the Burdigalian to the end of the Serravallian (Boudagher-Fadel and Lokier 2005; Sharaf et al. 2005; Hallock et al 2006; Renema 2015). Its presence restricts the possible age of the interval to zones M9 to M10 (Fig. 8). However, according to Renema (2015), the morphology of the examined *C. annulatus* is quite primitive and closer to those of Burdigalian and Langhian specimens. Nonetheless, planktonic foraminifera and calcareous nannofossil distributions support the M9 to M10 hypothesis. The interval from Sample 8HCC to 71X-CC should span between the Zones M9 and M11 as defined

Table 1 Distribution of the identified species among the samples

Species	7H-CC	15F-CC	22F-CC	29F-CC	107X-CC	108X-CC	109X-CC	110X-CC
N. ex. interc. *ruttenii-martini*	X	X	X	X				
N. transiens			X	X				
N. ex. interc. *isolepidinoides-sumatrensis*					X	X		
C. annulatus	X	X	X	X				
C. eidae					X			
H. (*V.*) *borneensis*					X	X	X	
Heterostegina (*V.*) sp. 1							X	X
O. cf. *heterosteginoides*					X	X		
O. complanata				X			X	
Operculina sp. 1					X	X	X	X
Nummulitidae sp. 1	X	X	X	X				
A. lessonii	X	X	X	X				
A. mammilla					X	X	X	X
Sphaerogypsina sp. 1				X				
Sphaerogypsina sp. 2						X		

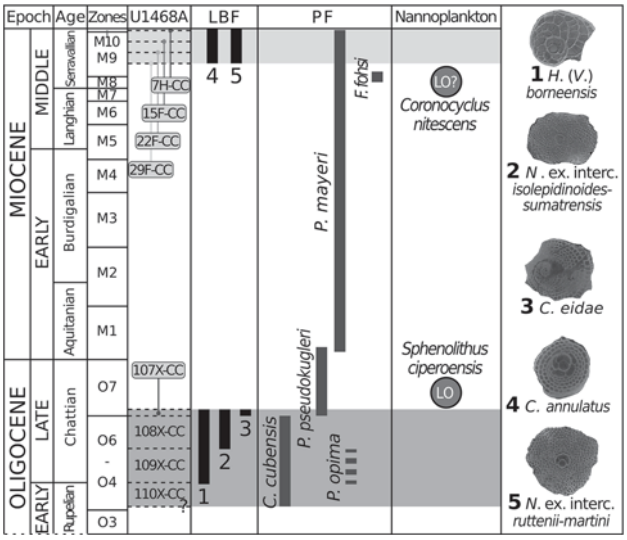

Fig. 8 Stratigraphic range of age-diagnostic LBF, planktonic foraminifera and calcareous nannofossils biostratigraphy from IODP359 Hole U1468A. Grey shading represents samples analyzed in this study and dashed lines reflect sample boundaries whereby the exact start or end points are uncertain. Planktonic foraminifera zones are from Wade et al. (2011). Planktonic foraminifera (PF) distribution is from Betzler et al. (2017) and Spezzaferri et al. (in prep.). Calcareous nannofossils distribution is from Betzler et al. (2017)

by the First Occurrence (FO) of *Fohsella fohsi* and Last Occurrence (LO) of *Paragloborotalia mayeri* (Fig. 8; Betzler et al. 2017; Spezzaferri et al. in prep.). Nannofossils distribution indicates a M5 to M12 age (Zones NN6 to NN15) for the interval 6H though 66X (Fig. 8; Betzler et al. 2017).

In the second interval (Units VII and VIII; Samples 107X-CC to 110X-CC) the majority of LBF are poorly preserved and fragmented, with extensive borings and authigenic mineral fillings. Sample 108X-CC, in particular, is dominated by fragments of lepidocyclinids, probably produced by the breakage of individuals with a prominent equatorial flange (the observed fragments have equatorial chambers arranged in an intersecting curved pattern similar to that of *N.* ex. Interc. *isolepidinoides-sumatrensis*). The LBF assemblage is more varied and diverse than in the first interval (Table 1). Sample 107X-CC is characterized by *Nephrolepidina* ex. interc. *isolepidinoides-sumatrensis* (closer to the *N. sumatrensis*-type), *Heterostegina* (*Vlerkina*) *borneensis*, and *Cyclocypeus eidae* (Table 1; Fig. 8). This assemblage suggests a late Oligocene age, equivalent to Zone O7 (Fig. 8; Adams 1970; Van Vessem 1978; Chaproniere 1984; Boudagher-Fadel and Lord 2000; Hallock et al. 2006; Sharaf et al. 2005; Lunt and Renema 2014). In Sample 108X-CC *N.* ex. interc. *isolepidinoides-sumatrensis* is closer to the *N. isolepidinoides* type. The assemblage includes also *H.* (*V.*) *borneensis*, while *C. eidae* is no longer present (Table 1; Fig. 8). This association is suggestive of an older age than Sample 107X-CC, ranging from Zones O4 to O7 (Chaproniere 1984; Van Vessem 1978; Boudagher-Fadel and Lord 2000; Sharaf et al. 2005; Lunt and Renema 2014). The only biostratigraphic marker in Sample 109X-CC is *H.* (*V.*) *borneensis* (Table 1; Fig. 8). The specimens still present alar prolongations divided into chamberlets, pointing toward a late Oligocene age (Lunt and Renema 2014). The presence of *Heterostegina* (*V.*) sp. 1 (more primitive than *H.* (*V.*) *borneensis* because of its higher X value and lower S4+5 value) suggests this sample may be older than both 107X-CC and 108X-CC. No age-diagnostic LBF were recognized in the lowermost sample, making its placement uncertain (Table 1).

Planktonic foraminifera and calcareous nannofossil distributions are in agreement with the LBF stratigraphy. Sample 107X-CC can be allocated to Zone O7 due to the FO of *Paragloborotalia pseudokugleri*, while an older age is suggested for 108X-CC and 109X-CC due to the presence of *Chilogumbelina cubensis* and *Paragloborotalia opima* (Fig. 8; Spezzaferri et al. in prep.). Nannofossils indicate that Sample 107X is younger than 27.27 Ma and, therefore, younger than Zone O6 (Fig. 8; Betzler et al. 2017).

5.2 CT-scan and LBF biostratigraphy

By providing a large number of 3D models in short time, X-ray tomography proved to be an useful tool for LBF stratigraphy (especially in a context where samples are limited and destroying them is not an option). Approximately 12 h for scanning and 72 h for processing the raw data were necessary to produce all 160 models (the measurements entailed an additional 48 h of work). The major limitation to this approach seems to be the preservation of the specimens. Since CT-scan imaging is based on density contrast, secondary infilling of the chambers (e.g., sediment, cement or authigenic minerals), may jeopardize the results, in this instances traditional thin sections are probably more effective. Actually, due to the poor preservation of the material it was often impossible to resolve most of the chambers, especially for the nummulitids. However, exquisite results were obtained with lepidocyclinids which were well preserved. Since this group includes some of the most reliable age-diagnostic LBF, fast CT-scanning could significantly improve the knowledge on lepidocyclinids distribution, by mass-producing high-quality data and allowing non-destructive examination of the holotypes. Although our technique is fast and very good for the study of large chambers along the equatorial plane, it may not be perfect to investigate the fine structure of alar prolongations or the volume and the 3D shape of the chambers, which are potentially crucial for nummulitids evolutionary history (e.g., Cotton et al. 2015; Renema and Cotton 2015).

These elements, coupled with the study of growth-invariant parameters, are key elements for improving LBF taxonomy, phylogenesis and evolution (Hohenegger 2011; Renema and Cotton 2015). Nevertheless, our fast approach produced a reliable LBF-based stratigraphy that fits well with the available information on the distribution of both planktonic foraminifera and calcareous nannofossils. More detailed analyses of the lepidocyclinids, which are by far the most useful taxa in Hole U1468A, may refine the model and provide a powerful instrument for correlations. In this framework the use of independent age control systems, such as Strontium Isotope Stratigraphy, is crucial since planktonic foraminifera and calcareous nannofossils are rare in LBF-dominated intervals.

6 Conclusions

Large benthic foraminifera provided a reliable biostratigraphy for two shallow-water intervals in Hole U1468A. A late middle-Miocene age is suggested for Unit II and a late Oligocene age for Unit VII–VIII. These results are in agreement with the preliminary ages from planktonic foraminifera and calcareous nannofossils.

The evolution of the embryonic apparatus of *Nephrolepidina* appears to be an accurate biostratigraphic tool for this area. Further analyses focused on this genus will provide a powerful instrument to date these shallow-water deposits. The use of CT-scan proved to be valuable by producing non-destructive data in short time. This approach has the potential to advance biostratigraphy in shallow-water environments, opening new possibilities for paleontologists.

Acknowledgements We are grateful to the IODP for providing the samples used in this study. Christoph Neururer (Fribourg) is acknowledged for assistance during the CT scanning. Warm thanks to A. Collareta, W. Renema and J. Hohenegger for their useful suggestions. This study was supported by the Swiss National Science Foundation (200021_165852/1).

References

Adams, C. G. (1970). A reconsideration of the East Indian letter classification of the Tertiary. *Bulletin of the British Museum* (*Natural History*). *Geology, 19*(3), 85–137.

Aubert, O., & Droxler, A. W. (1996). Seismic stratigraphy and depositional signatures of the Maldive carbonate system (Indian Ocean). *Marine and Petroleum Geology, 13*(5), 503–536.

Banner, T. F., & Hodgkinson, L. R. (1991). A revision of the foraminiferal subfamily Heterostegininae. *Revista Espanola de Micropaleontologia, 13,* 101–140.

Beavington-Penney, S. J., & Racey, A. (2004). Ecology of extant nummulitids and other large benthic foraminifera in paleoenvironmental analysis. *Earth-Science Reviews, 67,* 219–265.

Benedetti, A., & Briguglio, A. (2012). *Risananeiza crassaparies* n. sp. from the Late Chattian of Porto Badisco (southern Apulia). *Bollettino della Società Paleontologica Italiana, 51,* 167–176.

Benedetti, A., Less, G., Parente, M., Pignatti, J., Cahuzac, B., Torres-Silva, A. I., et al. (2017). *Heterostegina matteuccii* sp. nov. (Foraminiferida: Nummulitidae) from the lower Oligocene of Sicily and Aquitaine: A possible transatlantic immigrant. *Journal of Systematic Palaeontology, 16,* 87–110.

Betzler, C., & Chaproniere, G.C.H. (1993). Paleogene and Neogene Larger Benthic foraminifera from the Queensland Plateau: biostratigraphy and environmental significance. *Proceedings of the Ocean Drilling Program, Scientific Results*. *133*, 51-66

Betzler, C., Lüdmann, T., Hübscher, C., & Fürstenau, J. (2013). Current and sea-level signals in periplatform ooze (Neogene, Maldives, Indian Ocean). *Sedimentary Geology, 290,* 126–137.

Betzler, C., Eberli, G.P., Alvarez Zarikian, C.A., Alonso-García, M., Bialik, O.M., Blättler, C.L., Guo, J.A., Haffen, S., Horozal, S., Inoue, M., Jovane, L., Kroon, D., Lanci, L., Laya, J.C., Ling Hui Mee, A., Lüdmann, T., Nakakuni, M., Nath, B.N., Niino, K., Petruny, L.M., Pratiwi, S.D., Reijmer, J., Reolid, J., Slagle, A.L., Sloss, C.R., Su, X., Swart, P.K., Wright, J.D., Yao, Z., Young, J.R. (2017). Site U1468. In Betzler, C., Eberli, G.P., Alvarez Zarikian, C.A., and the Expedition 359 Scientists, *Maldives Monsoon and Sea Level. Proceedings of the International Ocean Discovery Program, 35*9 (pp. 1-40). College Station, TX (International Ocean Discovery Program).

Boudagher-Fadel, M. K. (2002). The stratigraphic relationship between planktonic and larger benthic foraminifera in Middle Miocene to Lower Pliocene carbonates facies Sulawesi, Indonesia. *Micropalaentology, 48,* 153–176.

Boudagher-Fadel, M. K. (2008). Evolution and geological significance of Larger Benthic Foraminifera. *Elsevier Science, 21,* 544.

Boudagher-Fadel, M. K., & Banner, F. T. (1999). Revision of the stratigraphic significance of the Oligocene-Miocene "Letter Stages". *Revue de Micropaléontogie, 42*(2), 93–97.

Boudagher-Fadel, M. K., & Lokier, S. W. (2005). Significant Miocene larger foraminifera from South Central Java. *Revue de Paleobiologie, 24,* 291–309.

Boudagher-Fadel, M. K., & Lord, A. R. (2000). The evolution of *Lepidocyclina* (L.) *isolepinoides*, *L.* (*Nephrolepidina*) *nephrolepidinoides* sp. NOV., *L.* (*N.*) *brouweri* and *L.* (*N.*) *ferreroi* in the Late Oligocene-Miocene of the far East. *Journal of Foraminiferal Research, 30*(1), 71–76.

Briguglio, A., & Hohenegger, J. (2014). Growth oscillation in larger benthic foraminifera. *Paleobiology, 40,* 494–509.

Briguglio, A., Hohenegger, J., & Less, G. (2013). Paleobiological applications of three-dimensional biometry on larger benthic foraminifera: A new route of discoveries. *Journal of Foraminiferal Research, 43,* 67–82.

Briguglio, A., Wöger, J., Wolfgring, E., & Hohenegger, J. (2014). Changing investigation perspectives: methods and applications of computed tomography on larger benthic foraminifera. In H. Kitazato & J. Bernhard (Eds.), *Experimental Approaches in Foraminifera: Collection, Maintenance and Experiments* (pp. 55–70). Japan: Springer Environmental Science Series.

Briguglio, A., Kinoshita, S., Wolfgring, E., & Hohenegger, J. (2016). Morphological variations in *Cycloclipeus carpenteri*: Multiple embyos and multiple equatorial layers. *Palaeontologia Electronica*. https://doi.org/10.26879/595.

Chaproniere, G. C. H. (1980). Biometrical studies of early Neogene larger Foraminiferida from Australia and New Zealand. *Alcheringa, 4,* 153–181.

Chaproniere, G. C. H. (1984). The Neogene larger foraminiferal sequence in the Australian and New Zealand regions, and its relevance to the East Indies letter stage classification. *Palaeogeography Palaeoclimatology Palaeoecology, 46,* 25–35.

Cotton, L. J., Pearson, P. N., & Renema, W. (2015). A new Eocene lineage of reticulate *Nummulites* (Foraminifera) from Kilwa district, Tanzania; A place for *Nummulites ptukhiani*? *Journal of Systematic Palaeontology, 14,* 569–579.

Droxler, A.W., Haddad, G.A., Mucciarone, D.A., Cullen, J.L. (1990). Pliocene–Pleistocene aragonite cyclic variations in Holes 714A and 716B (The Maldives) compared with Hole 633A (The Bahamas): records of climate-induced CaCO3 preservation at intermediate water depths. In Duncan, R.A., Backman, J., Peterson, L.C., et al., (Eds.), *Proceedings of the Ocean Drilling Program*, *Scientific Results*, *115*, (pp. 539–577). College Station, TX (Ocean Drilling Program).

Hallock, P. (1981). Production of carbonate sediments by selected large benthic foraminifera on two Pacific coral reefs. *Journal of Sedimentary Petrology, 51,* 467–474.

Hallock, P., Sheps, K., Chaproniere, G., Howell, M. (2006). Larger benthic foraminifera of the Marion Plateau, Northeastern Australia (ODP Leg 194): Comparison of faunas from bryozoans (Sites 1193 and 1194) and red algal (Sites 1196-1198) dominated carbonate platforms. In Anselmetti FS, Blum P and Betzler C (Eds.), *Proceedings of the Ocean Drilling Program*, *Scientific Results*, *194*, (pp. 1–31). College Station, TX (Ocean Drilling Program).

Haynes, J. R. (1965). Symbiosis, wall structure and habitat in foraminifera. *Contributions from the Cushman Foundation for Foraminiferal Research, 16,* 40–43.

Hohenegger, J. (1994). Distribution of living larger Foraminifera NW of Sesoko-Jima, Okinawa, Japan. *Marine Ecology, 15,* 291–334.

Hohenegger, J. (2000). Coenoclines of larger foraminifera. *Micropaleontology, 46,* 127–151.

Hohenegger, J. (2011). Growth-invariant meristic characters tools to reveal phylogenetic relationships in Nummulitidae (Foraminifera). *Turkish Journal of Earth Sciences, 20,* 655–681.

Hohenegger, J., & Briguglio, A. (2014). Methods for estimating growth pattern and lifetime of foraminifera based on chamber volumes. In H. Kitazato & J. Bernhard (Eds.), *Experimental Approaches in Foraminifera: Collection, maintenance and experiments* (pp. 29–54). Japan: Springer.

Hohenegger, J., Yordanova, E., & Hatta, A. (2000). Remarks on West Pacific Nummulitidae (Foraminifera). *Journal of Foraminiferal Research, 30,* 3–28.

Hottinger, L. (1977). Foraminifères operculiniformes. *Mémoires du muséum National d'Histoire Naturelle, Paris, Nouvelle Série, Série C, 40,* 1–159.

Hottinger, L. (1983). Reconstruction of marine paleoenvironments. In Meulenkamp J. E. (Ed.), *Processes determining the distribution of foraminifera in space and time*. *Utrecht Micropaleontological Bulletin, 30*, 239–253.

Langer, M. R., & Hottinger, L. (2000). Biogeography of selected "larger" foraminifera. *Micropaleontology, 46,* 105–126.

Lee, J. J., & Hallock, P. (1987). Algal symbiosis as a driving force in the evolution of larger Foraminifera. *Annals of the New York Academy of Sciences, 503,* 330–347.

Less, G., Özcan, E., Papazzoni, C. A., & Stockar, R. (2008). The middle to late Eocene evolution of nummulitid foraminifer *Heterostegina* in the Western Tethys. *Acta Palaeontologica Polonica, 53,* 317–350.

Loeblich, A. J. R., & Tappan, H. (1964). Sarcodina chiefly "The camoebians" and Foraminiferida. In R. C. Moore (Ed.), *Treatise on Invertebrate Paleontology, part C, 1–2* (pp. 1–900). Lawrence: Geological Society of America and University of Kansas Press.

Lunt, P., & Renema, W. (2014). On the *Heterostegina-Tansinhokella-Spiroclypeus* lineage(s) in SE Asia. *Berita Sedimentologi Indonesian Journal of Sedimentary Geology, 30,* 6–31.

Matteucci, R., & Schiavinotto, F. (1977). Studio biometrico di *Nephrolepidina*, *Eulepidina* e *Cycloclypeus* in due campioni dell'Oligocene di Monte La Rocca, L'Aquila (Italia centrale). *Geologica Romana, 16,* 141–171.

Matteucci, R., & Schiavinotto, F. (1980). Ricerche biometriche su *Operculina GR. Alpina* Douvillé. *Geologica Romana, 19,* 251–265.

O'Herne, L. (1972). Secondary chamberlets in *Cycloclypeus*. *Scripta Geologica, 7,* 1–35.

Özcan, E., Less, G., Báldi-Beke, M., Kollányi, K., & Acar, F. (2009). Oligo-Miocene foraminiferal record (Miogypsinidae, Lepidocyclinidae and Nummulitidae) from the Western Taurides (SW Turkey): Biometry and implications for the regional geology. *Journal of Asian Earth Sciences, 34,* 740–760.

Pignatti, J., Samso, J. M., Schaub, H., Sirel, E., Strougo, A., Tambareau, Y., et al. (1998). Larger foraminiferal biostratigraphy of the Tethyan Paleocene and Eocene. *Bulletin Societé Géologie de France, 169,* 281–299.

Renema, W. (2006). Large benthic foraminifera from the deep photic zone of a mixed siliciclastic-carbonate shel off East Kalimantan, Indonesia. *Marine Micropaleontology, 58,* 73–82.

Renema, W. (2007). Fauna Development of Larger Benthic Foraminifera in the Cenozoic of Southeast Asia. In W. Renema (Ed.), *Biogeography, time and place: distributions, barriers and islands* (pp. 179–215). Dordrecht: Springer.

Renema, W. (2015). Spatiotemporal variation in morphological evolution in the Oligocene-recent larger benthic foraminifera genus Cycloclypeus reveals geographically undersampled speciation. *GeoResJ, 5,* 12–22.

Renema, W. (2018). Terrestrial influence as a key driver of spatial variability in large benthic foraminiferal assemblage composition in the Central Indo-Pacific. *Earth Sciences Review, 177,* 514–544.

Renema, W., & Cotton, L. (2015). Three dimensional reconstructions of Nummulites tests reveal complex chamber shapes. *PeerJ, 3,* e1072. https://doi.org/10.7717/peerj.1072.

Renema, W., Hoeksema, B. W., & van Hinte, J. E. (2001). Larger benthic foraminifera and their distribution patterns on the Spermonde shelf, South Sulawesi. *Zoologische Verhandelingen, Leiden, 334,* 115–149.

Schaub, H. (1981). Nummulites et Assilines de la Thethys paléogène. Taxonomie, phylogénèse, biostratigraphie. *Mémoires Suisses de Paléontologie, 104–106,* 1–236.

Schiavinotto, F. (1978). Nephrolepidina nella Valle del Maso (Borgo Valsugana-Italia settentrionale). *Rivista Italiana di Paleontologia e Stratigrafia, 84,* 729–750.

Serra-Kiel, J., Hottinger, L., Caus, E., Drobne, K., Fernandez, C., Jauhri, A. K., et al. (1998). Larger foraminiferal biostratigraphy of the Tethyan Paleocene and Eocene. *Bulletin de la Société Géologique de France, 169,* 281–299.

Sharaf, E. M., Boudagher-Fadel, M. K., Simo, J. A., & Carroll, A. R. (2005). Biostratigraphy and strontium isotope dating of Oligocene-Miocene strata, East Java, Indonesia. *Stratigraphy, 2*(3), 239–258.

Tan, S. H. (1932). On the genus *Cycloclypeus* Carpenter. Part I, and an appendix on the *Heterostegines* of Tjimanggoe, S. Bantam, Java. *Wetenschappelijke Mededeelingen Dienst van den Mijnbouw in Nederlandsch-Indië, 19,* 3–194.

Torres-Silva, A. I., Hohenegger, J., Ćorić, S., & Briguglio, A. (2017). Biostratigraphy and evolutionary tendencies of Eocene heterostegines in Western and Central Cuba based on morphometric analyses. *Palaios, 32,* 44–60.

Tudhope, A.W. & Scoffin, T.P. (1988). The relative importance of benthic foraminifera in the production of carbonate sediment on the Central Queensland shelf. *Proceedings of the 6th International Coral Reef Symposium, Australia, 2*, 583–588.

Van der Vlerk, I. M. (1959). Modifications de l'ontogénèse pendant l'évolution des Lépidocyclines (Foraminifères). *Bulletin de la Société Géologique de France Notes et Mémoires Série, 7*(1), 669–673.

Van der Vlerk, I. M. (1963). Biometric research on *Lepidocyclina*. *Micropaleontology, 9,* 425–426.

Van der Vlerk, I. M., & Umbgrove, J. H. L. (1927). Tertiaire gidsforaminiferen uit Nederlandsch Oost-Indie. *Wetenschappelijke Mededeelingen, Dienst Mijnbouw Bandoeng, 6,* 1–31.

Van Vessem, E. J. (1978). Study of Lepidocyclinidae from South-East Asia, particularly from Java and Borneo. *Utrecht Micropalaeontological Bullettin, 19,* 1–163.

Wade, B. S., Pearson, P. N., Berggren, W. A., & Pälike, H. (2011). Review and revision of Cenozoic tropical planktonic foraminiferal biostratigraphy and calibration to the geomagnetic polarity and astronomical time scale. *Earth Science Reviews, 104,* 111–142.